

INVESTIGATION OF UNIVERSALLY ELECTRIC PROPULSION SYSTEMS FOR TRANSPORT AIRCRAFT

**Patrick C. Vratny, Philipp Forsbach, Arne Seitz, Mirko Hornung
Bauhaus Luftfahrt e.V. Munich, Germany**

Keywords: *electric motor, high temperature superconducting, motor controller,
electric propulsion, cryocooler*

Abstract

Hybrid electric as well as universally electric aircraft are promising approaches fulfilling the targeted emission improvements stipulated by the NASA N+3 goals and the European Strategic Research Innovation Agenda. For high power applications required in transport category aircraft high-temperature superconducting (HTS) motors seem to be a key technology for which accurate mass and efficiency models are required. This paper introduces a comprehensive mass and efficiency estimation approach for full HTS motors including also the estimation of the required inverter and cooling system devices. Finally, the applicability of the HTS motor sizing and performance model to a ducted fan propulsion system featuring 22.2MW take-off power is demonstrated. An optimal motor design for this power range was identified at 11000 rpm with a specific power of 15.8 kW/kg at 99.2% efficiency and controller design with 23 kW/kg and over 99.5% efficiency. The demonstrated approach serves as baseline for further investigations of optimized electric motor design driving a ducted fan for different thrust and power ranges. Furthermore, analysis has shown that the electric motor geometrical model for rotor and stator has to be refined for different pole pairs.

1 Introduction

Ambitious emission reduction goals, unveiled by notable organizations like the NASA with the NASA N+3 goals [1] or the European Commission with the Strategic Research Innovation Agenda (SRIA) [2], are confronting the aviation community with new challenges in aircraft design. Those goals are targeting significant emission and noise reductions for future transport aircraft.

One possibility could be based on the electrification of the aircraft subsystems partially already shown with the Boeing 787. Beyond the electrification of subsystems, in particular, the electrification of aircraft propulsion power has shown significant possible fuel reduction potential. A multitude of concepts and studies were already published in the recent past considering all-electric and hybrid-electric propulsion systems[1][3][4]. All these concepts require a propulsion system, which is able to handle high power demands in the range of megawatts necessary for operating a transport category aircraft within the flight envelope.

This paper will give a stronger insight in the design of the electric components directly involved in an electric propulsion system and investigating the sizing impacts and strategies of these electric components. The focus lies on the design of an optimal electric motor and corresponding controller architecture with regard to efficiency and mass for universally-electric, but also valid for hybrid electric, aircraft. For that reason a ducted fan is equipped with an electric motor to find the optimal ratio

of fan speed to motor speed with respect to mass and efficiency.

2 Overview of Electric Components

The following section gives an overview of different electric motors, converters and controllers already used in all-electric and hybrid-electric vehicles.

2.1 Electric Machines

Electric machines are required to convert electric energy (with the help of magnetic and electric fields) into mechanical energy to drive for example a propulsive device. The following section gives a brief overview of the basic functional principles and types of electric motors.

2.1.1 Fundamentals of Electric Motors

An electric motor consists of several mechanical parts. The rotor comprises a shaft to transmit torque and rotational speed, and, the rotor core and the rotor armature, which are responsible for the generation of an electromagnetic field (EMF) acting against the stator field. In case of a permanent magnet motor the rotor armature is replaced by permanent magnets. The stator consists of slots and teeth holding the stator armature. The stator armature is assisted by the surrounding stator core. This core increases the electromagnetic effects generated by the armature. Between the rotor and the stator is a geometrically imposed small air gap. This air gap is mechanical necessary to allow the rotor to move, but has also an important impact to the electromagnetic performance of the motor. For electric vehicles an electronic control unit is required to control the supply of correct voltage, amount of electric current and also prescribe the frequency to control required torque, T , and rotational speed, n , within the operational envelope. Those parameters have a significant impact on the motor efficiency, η , of the electric machine. The most important parameters for designing an electric machine are marked in the qualitative T-n-diagram in Fig. 1. The sizing point P_{Design} is equivalent to the power demand

during the one engine inoperative case for aircraft design [5].

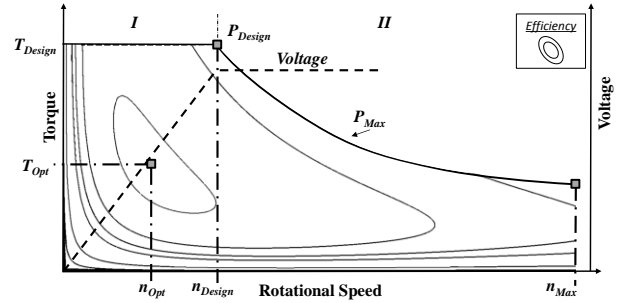


Fig. 1: Design chart of an electric machine showing important design points.

The design chart shown above is normally divided into two regions. Region I is equivalent to the constant torque section, where the power increases with increasing rotational speed, and, Region II represents the constant power section, where the torque decreases with increasing rotational speed, also known as flux-weakening region. The peak power of the electric motor can be determined with the fundamental equation (1):

$$P_{Design} = N \cdot B \cdot A \cdot I \cdot \omega_{Motor} = T \cdot \omega_{Shaft} \quad (1)$$

Here N represents the number of windings of one coil, B the magnet flux density, A the conductor area of a winding, I the electric current and the motor angular velocity, ω_{Motor} , which can be unequal to the mechanical rotational speed ω_{Shaft} (depending on the number of pole pairs). From this equation the torque can also be written in the form as shown in equation (2) including the coil length, l :

$$T = N \cdot B \cdot A \cdot I = \frac{A}{l} \cdot N^2 \cdot I^2 \quad (2)$$

By linking the magnetic flux density, B , with the magnetic field strength, H , and the permittivity, μ , as shown in equation (3), it can be seen that the torque only depends upon the square of the electric current in the first region for a given motor type.

$$B = \mu \cdot H = \frac{I \cdot N}{l} \quad (3)$$

Besides the electric current also the voltage, u , is an important design parameter and can be determined with equation (4):

$$u = -N \cdot \frac{d\varphi}{dt} \quad (4)$$

$$U_{max} = \varphi \cdot N \cdot \omega_{Motor}$$

With $\varphi = B \cdot A$

The voltage, u , depends on the number of windings, N , per coil and the change of the magnetic flux, φ . The maximum voltage, U_{max} , depends then mainly on B and ω_{Motor} . When U_{max} is reached, the motor speed can only be further increased when φ is decreased (this is also known as flux weakening). Because A is fixed for a certain motor, the decreasing of the magnetic flux can only be achieved by decreasing the magnetic flux density via the electric current according to equation (3). This in turn has an impact on the available torque output, which is also decreasing. Finally, when combining equations (1)-(4) scaling factors for I , U and B can be derived and can be set in correlation with T and n as shown in Table 1.

Table 1: Scaling relations of electric motors for region I and II

	Region I of Fig. 1	Region II of Fig. 1
Voltage U	\sqrt{T}, n	<i>const.</i>
Current I	\sqrt{T}	
Flux field φ, B	\sqrt{T}	$\frac{1}{n}$

These scaling factors are based upon general relations that have to be adapted to different motor architectures. For the generation of the required electromagnetic forces, different motor architectures are available. The most common electric motor types for electric and hybrid vehicles are listed in Table 2. Here, Asynchronous Motors (ASM), Switched Reluctance Motors (SRM) and Permanent Magnet Synchronous Motors (PSM) machines are assessed according to their advantages and disadvantages as taken from Neudorfer [6].

Table 2: Overview of electric motors used in electric/hybrid vehicles. Based on [6]

Electric Motor	ASM	SRM	PSM
<i>Efficiency</i>	0	0	+3
<i>Mass</i>	0	0	+1
<i>Torque density</i>	0	+1	+3
<i>Inverter Complexity</i>	0	-3	-1

-3 strongly negative; -1 negative; 0 neutral; +1 positive; +3 strongly positive

Based on Table 2 PSM offer high energy and good mass efficiency and seem to be the most suitable motor type for aviation. Therefore, the focus in this paper will lie on PSMs also in view of future high temperature superconducting applications. The design of a PSM is similar to the ASM. The stator design (which is nearly identical to the ASM) consists of slots housing the windings, which are supplied by an external power source. The rotor normally consists of permanent magnets (PM) like Neodymium-Iron-Boron (NdFeB) instead of windings. This design requires an active power control unit which controls the electric current in the stator windings in a way that the poles of the rotor are always interacting with the stator EMF. This switching of the stator windings is linked to the motor frequency. Because the magnetic field of PMs is always available and no EMF has to be induced in the rotor windings required in an ASM design, the rotor can rotate at the same frequency as the stator winding supply. The brushless PSM design is also characterized as both reliable, and, particularly efficient because the rotor losses are nearly zero and the efficiency is about 95% [7].

2.1.2 High Temperature Superconducting

Superconducting is a physical effect where a certain group of materials lose their ohmic resistance at a specific temperature. It differs between low temperature (around 5K) and high temperature superconductors (HTS) operating between 60-77K [8]. In electric motor design this effect can be used to increase the electric field capability and also to increase the electric current density of the armature. Current motor designs are investigated where one part of the electric motor (either stator or rotor armature) is replaced by HTS coils. This leads to a specific power of up to 10 kW/kg running at 35,000 rpm [9]. Beyond that, in full HTS motors, both stator and rotor armatures are replaced by HTS material. With this configuration a specific power of up to 40 kW/kg (without cooling) may be achieved with efficiencies greater than 99% [10]. A disadvantage of the HTS motor is currently the cooling system, which requires cryocoolers to keep the HTS material at required temperature. These cryocoolers have

currently a specific power of about 0.33 kW/kg (with regard to input power) and a Carnot efficiency of 15% [10]. The goal here is to reach 30% Carnot efficiency [11].

2.2 Inverter and Controller

An inverter is required to change the electric current type, for example from direct current (DC) at input to an alternating current (AC) at output, in order to control an electric motor. Also a change in output frequency and voltage is mandatory to control the rotational speed. In case of a DC input the voltage source (or pulse control) inverter is commonly used to generate a three phase AC voltage. The most common architecture is the voltage source inverter shown in Fig. 2.

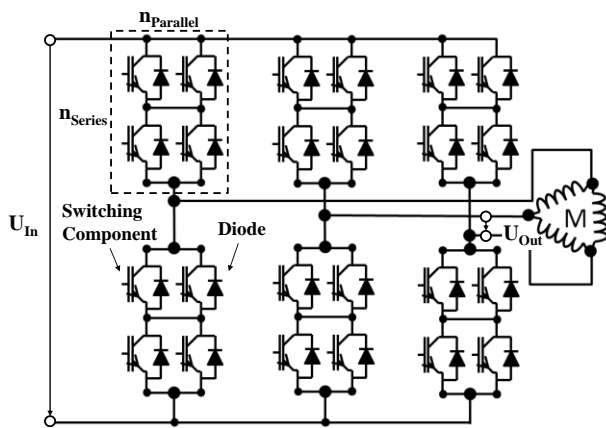


Fig. 2: Voltage Source Inverter for control of a 3-phase electric motor

The main components of this inverter are switching components and diode rectifiers, which can be grouped and connected in series (n_{Series}) and/or parallel ($n_{Parallel}$) according to operating voltage, U_{In} , electric current and redundancy aspects. The electric current is controlled by these modules in such a way that the coils of the electric motor, M , can be energized in positive as well as in a negative electric current direction. This depends upon whether a module is in a conducting or in a blocking mode. This leads to an electric field, which interacts or counteracts with the rotor field depending on the electric motor state. The aim of the switching elements is to control the current in a way that the output current approximates the required output sinusoidal

current waveform for the electric motor as close as possible. This requires a switching frequency which is higher than the motor frequency. There are different types of switching elements available depending on the switching frequency, voltage and power summarized in Table 3 given by [12]. For example, Metal-Oxide Semiconductor Field Effect Transistors (MOSFET) can switch at high frequency but at relative low power, while thyristors are able to switch at high power but at low frequency. The Insulated Gate Bipolar Transistors (IGBT) are somewhere between MOSFETs and thyristors. For the power and frequency range of an aircraft the IGBTs seem to be the most suitable.

Table 3: Overview of switching components based on [12]

	Current	Voltage	Frequency
MOSFET	0-250 A	Up to 1 kV	0-1 MHz
IGBT	0-2000 A	Up to 4 kV	1-10 kHz
Thyristor mainly AC/AC	0-2500 A	Up to 5 kV	< 1 kHz

A simple method to control the switching elements is done via pulse width modulation (PWM). For that reason the electric current is chopped via switching elements controlled by a microcontroller. Depending on the timely length of a pulse the voltage as well as the current can be controlled. In case of an electric current this is necessary to approximate the sinusoidal waveform of the electric current required for the motor coils.

3 Electric Component Modeling

In the following section the modeling approach of the performance and mass of conventional designed PSM as well as full HTS Motors is described. Furthermore, the performance and mass modelling of the inverter and the cryocooler is presented.

3.1 Electric Motor Model

This section describes an approach of scaling an existing motor to different power ranges to determine the mass and efficiency of the scaled motor type.

3.1.1 Geometry Modeling

The geometry is estimated based on methods published by Pyrhönen [13] and Rucker [14]. The principle geometric design, including major design parameters, is sketched in Fig. 3. The sleeve is not considered during the electric motor sizing.

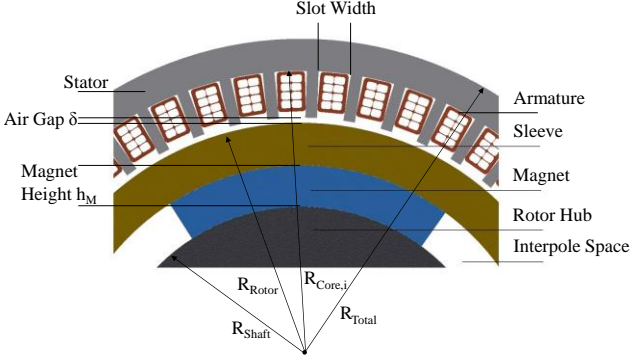


Fig. 3: Principle geometric design of the electric motor based on [15]

The total rotor diameter D_{Rotor} is estimated with equation (5):

$$D_{Rotor} = D_{Shaft} + 2 \cdot (h_M + \delta) \quad (5)$$

D_{Shaft} represents the effective diameter responsible for the required torque. This parameter is an input parameter and optimized during the electric motor sizing. The parameter h_M represents the magnet height established according to methods published by Bongomolov [15]. The air gap, δ , the distance between rotor magnets and stator, is calculated with equation (6) according to Pyrhönen [13]:

$$\delta = \frac{C_1 + C_2 \cdot p^{0.4}}{1000} [m] \quad (6)$$

The parameters C_1 and C_2 are dependent on the number of pole pairs and can be determined by Table 4 also taken from [13].

Table 4: Air gap parameters

	C_1	C_2
One Pole Pair	0.2	0.01
Pole Pairs greater than 1	0.18	0.006

D_{Shaft} is limited by a maximum centrifugal force according to equation (7) taken from [13]:

$$R_{p,0.2} \geq k \cdot \rho \cdot \pi^2 \cdot n_{max}^2 \cdot D_{Shaft}^2 \quad (7)$$

$R_{p,0.2}$ is the maximum yield strength of rotor material, n_{max} the maximum rotational speed of

the rotor with the shaft diameter D_{Shaft} (two times R_{Shaft}). The required rotor length is estimated with equation (8):

$$L_{Rotor} = \frac{P_{Design}}{D_{Shaft} \cdot \pi^2 \cdot n \cdot \sigma} \quad (8)$$

Here, σ is the available shear stress acting on the rotor surface in units of N/m². The available shear stress can be calculated with equation (9) according to [13].

$$\sigma = J \cdot \frac{1}{\sqrt{2}} \cdot B \cdot \left(\frac{D_{Shaft}}{D_{Ref}} \right)^{0.25} \quad (9)$$

σ is a function of the air gap current density J , B and the shaft diameter. Finally, the total electric motor diameter can be calculated with equation (10):

$$D_{Total} = D_{Core,i} + \frac{k_{Stator_Yoke}}{p} \cdot D_{Rotor} \quad (10)$$

The total diameter D_{Total} is dependent on the inner core diameter $D_{Core,i}$, the stator yoke ratio k_{Stator_Yoke} and the number of pole pairs, p , times the rotor diameter, D_{Rotor} , which represents the core depth. $D_{Core,i}$ is calculated with equation (11) including the slot depth d_{Slot} :

$$D_{Core,i} = D_{Rotor} + 2 \cdot d_{Slot} \quad (11)$$

The total machine length can then be defined with equation (12):

$$L_{Total} = L_{Rotor} + 2 \cdot \frac{L_{Coil,End}}{2 \cdot \pi} \quad (12)$$

The length of an end coil, $L_{Coil,End}$, is directly calculated according to methods described in Rucker [14] and not further stated in this paper. The maximum rotor length L_{Rotor} can be calculated with equation (13) according to Pyrhönen [13]:

$$L_{Rotor,max} = k_{Length} \cdot \sqrt{\frac{\pi^2}{k \cdot 2\pi \cdot n_{max}} \cdot \sqrt{\frac{E \cdot I}{\rho \cdot A}}} \quad (13)$$

The rotor length is limited by the maximum rotational speed, n_{max} , the rotor young's modulus, E , and rotor density, ρ , as well as the rotor area, A , and mass moment of inertia, I (full shaft considered). The parameter k represents an additional safety factor according to Table 5 and k_{Length} reduces the theoretically maximum length

by one third according to [13] to consider also bearing mountings, slits, etc. Furthermore, the rotor length can also be limited due to installation space. Table 5 summarizes the main design parameters for all motor designs mainly taken from [14].

Table 5: Constant parameters for all motor designs with one pole pair mainly based on Rucker [14]

Parameter	Value	Parameter	Value
Number of phases	3	Stator/Rotor density [kg/m ³]	7860/4800[16]
Number of pole pairs p	1	Rotor young's modulus E [N/m ²]	210x10 ⁹
Number of coils N	48	Rotor tensile strength $R_{p,0.2}$ [N/m ²]	250x10 ⁶
Magnet angle [deg]	50	Stator yoke ratio [-] $k_{Stator-Yoke}$	0.6
Mass service fraction $k_{Services}$ [17]	0.13	Safety factor k	1.5

Table 6 gives an overview of parameters used for conventional PSM and full HTS motor design. For full HTS motor a slotless motor configuration is assumed [18].

Table 6: Parameters used for conventional and full HTS motor designs

	Conventional	Full HTS
Air gap current density J [A/m]	65000	130000*
Magnet flux density B [T]	1.05	2.0 [11]
<i>Additional parameters used for geometry and mass method published by Rucker [14]</i>		
Magnet density [kg/m ³]	7400	6500
Armature density [kg/m ³]	8900	6500
Armature current density [A/m ²]	2.5·10 ⁶	100·10 ⁶
Number of slots	36	0 [18]
Number of slots short pitched	1	
Slot depth [m]	0.025	
Slot depression depth [m]	0.0005	
Slot depression width [m]	10 ⁻⁶	
Peripheral tooth fraction	0.5	
* based on a liquid water cooled stator according to Pyrhönen [13]		

3.1.2 Mass Modeling

Based on the geometry data calculated in the previous section, the mass for each component is calculated using the method published by

Rucker [14]. The total machine weight is the sum of all components as shown with equation (14):

$$m_{Motor} = \sum_n m_n \quad (14)$$

For each electric motor component the volume is calculated and multiplied with the corresponding material density. It includes the rotor mass m_{Rotor} , the magnet mass $m_{Magnets}$ (for HTS motors corresponding HTS coils are considered), the stator mass m_{Stator} (including teeth and stator core mass) and the armature mass m_{Arm} in the stator. For a consideration of the frame and mounting masses, $m_{Services}$, of an electric motor Lokhandwalla et.al [17] recommend a service mass factor, k_m , of 13% of the total machine weight as shown in equation (15):

$$m_{Services} = k_m \cdot (m_{Rotor} + m_{Stator} + m_{Magnets} + m_{Arm}) \quad (15)$$

3.1.3 Efficiency Modeling

This section describes the modelling approach of the conventional as well as the HTS motor. The efficiency model to determine the design and off-design characteristics of the electric motor is based on reference values. The shown data in Table 7 are based on a HTS motor design by [19] and can be adapted according to literature values for conventional motors. For example the core losses for a conventional motor are 4 times higher than for a HTS motor [20].

Table 7: Reference data of 1.0MW HTS electric motor at 1800 rpm used for efficiency calculation and based on [19]

Losses	Reference Losses	Percentage
Stator Core*, $P_{L,Ref,Core}$	11465 W	31.3%
Armature I ² R**, $P_{L,Ref,Arm}$	12429 W	33.9%
Stray Load**, $P_{L,Ref,Stray}$	1305 W	3.6%
Windage and Friction, $P_{L,Ref,Fri}$	1027 W	2.8%
Field Coil Cooling	7500 W	20.5%
Miscellaneous, $P_{L,Ref,Mis}$	2953 W	8.0%
* for conventional motors 4 times higher according to [20]		
** armature losses set to zero for full HTS motors, stray load losses reduced by 50%		

The core losses of the stator represent losses within the core material due to remagnetization (hysteresis) effects. The stator armature losses are caused by electric current due to the ohmic resistance. The windage and friction losses are caused by the rotor due to air friction and bearings. Finally, the so called miscellaneous losses include secondary effects due to geometry impacts such as stray load losses at mountings. The motor efficiency η_{Motor} can be calculated with equation (16) for each operational point of the electric motor summing up all individual losses.

$$\eta_{Motor} = \frac{P_{Out}}{P_{In}} = \frac{P_{Shaft}}{P_{Shaft} + \sum_n P_{Loss,n} + P_{Cryo}} \quad (16)$$

The loss calculation for the efficiency estimation of the electric motor design is based on the reference losses shown in Table 7 above. For that reason each loss category is initially scaled with the power ratio of the new design power P_{Design} to the reference power P_{Ref} as shown in equation (17).

$$k_{Scale} = \frac{P_{Design}}{P_{Ref}} \quad (17)$$

The core losses are mainly scaled with the electric current with the power of 1.353 [21], which is according to Table 1 equal to the square root of the torque, and the frequency ratio, which is equal to the rotational speed ratio. This approach is shown in equation (18):

$$P_{Loss,Core} = k_{Scale} \cdot P_{L,Ref,Core} \cdot \left(\frac{T}{T_{Design}} \right)^{1.353} \cdot \frac{n}{n_{Design}} \quad (18)$$

The armature losses (calculated with equation (19)) are only depending on the torque, which corresponds to I^2R , while it is assumed that the ohmic resistance R is constant over the entire motor envelope.

$$P_{Loss,Arm} = k_{Scale} \cdot P_{L,Ref,Arm} \cdot \frac{T}{T_{Design}} \quad (19)$$

The stray load losses depend, according to Grune [21], on the square of the magnetic flux ratio and the square of the rotational speed ratio. The magnetic flux according to Table 1 depends on the torque. Therefore, the stray load losses can be estimated with equation (20):

$$P_{Loss,Stray} = k_{Scale} \cdot P_{L,Ref,Stray} \cdot \frac{T}{T_{Design}} \cdot \left(\frac{n}{n_{Design}} \right)^2 \quad (20)$$

The air friction loss, which occur in the air gap, is calculated with equation (21) according to [22]:

$$P_{Loss,Air} = 1.7 \cdot \rho_{air} \cdot D_{Shaft}^4 \cdot L_{Rotor} \cdot n^3 \cdot \left(\frac{\pi \cdot D_{Shaft} \cdot \pi \cdot \delta}{v_{air}} \right)^{-0.15} \quad (21)$$

It depends on D_{Shaft} , L_{Rotor} , n , δ , and the air condition within the air gap with air density, ρ_{air} , and the kinematic viscosity, v_{air} . In HTS motors, the air friction losses can normally be neglected, because the air gap is evacuated due to insulation reasons [18]. The friction losses, which occur in the bearings only depend on the rotational speed and can be calculated with equation (22):

$$P_{Loss,Fri} = k_{Scale} \cdot P_{L,Ref,Fri} \cdot \left(\frac{n}{n_{Design}} \right) \quad (22)$$

Due to geometric considerations and additional stray load losses at mountings of the electric motor so called additional losses are occurring during the operation of an electric motor. These losses are mainly dependent on I^2 (equal to torque ratio according to Table 1) and the rotational speed as shown in equation (23) according to [21]:

$$P_{Loss,Misc} = P_{L,Ref,Misc} \cdot \frac{T}{T_{Design}} \cdot \left(\frac{n}{n_{Design}} \right)^{1.25} \quad (23)$$

The field coil cooling losses P_{Cryo} , also shown in Table 7, are not directly estimated in the motor efficiency calculation. This additional required cooling power demand for HTS motors is calculated separately, shown in the next section.

3.2 Cryo-Cooler Model

HTS technology requires an operational temperature of around 77K according to Brown [11]. For that reason cryocoolers are used, which cool the HTS motors. The required cooling power, $P_{Cooling}$, is determined with equation (24):

$$P_{Cooling} = P_{Motor} \cdot (1 - \eta_{Motor}) \cdot k_C \quad (24)$$

P_{Motor} is the actual motor power and η_{Motor} represents the current efficiency of the HTS motors determined by methods described in the previous section. The parameter k_C represents the fraction of heat dissipated to the HTS coils. According to Table 7 (previous page) it is assumed that only the armature losses of a HTS motor (only rotor coils) are responsible for a heating within the rotor. From the approximate 34% armature losses it is assumed that only 25% (inside area of armature) are responsible for the HTS coil heating. The required cryocooler power is then estimated with equation (25) according to Seitz et.al. [23]:

$$P_{Cryo} = P_{Cooling} \cdot \frac{C_{Carnot}}{\eta_{Cryo}} = P_{Cooling} \cdot \frac{(T_{sink} - T_{load})}{T_{load} \cdot \eta_{Cryo}} \quad (25)$$

T_{sink} is the surrounding temperature (assumption at ISA +10K conditions), T_{load} represents the operational temperature of the HTS motors and cables and η_{Cryo} represents the cryocooler efficiency based on the Carnot efficiency of 30% according to Brown [11]. The mass of the cryocooler is estimated with a specific power of 0.33 kW/kg according to Brown [11] and the maximum occurred cooling power calculated with equation (24).

3.3 Inverter and Controller Model

Based on Section 2.2 the following section describes the efficiency and mass modelling of a voltage source inverter used for the control of the electric motor.

3.3.1 Efficiency Modeling

The inverter was modelled to estimate the efficiency within the required power range of the electric motor. The loss model is based on an existing power switch using scaling dependencies for the efficiency estimation similar to the electric motor model, which are based on Wintrich et.al. [24]. The following assumptions were made to the model

- switching times are neglected
- temperature is set constant to 313K (100°C)

- switching frequency ripple of the AC current is neglected
- switching frequency is orders of magnitude higher than output frequency
- linear modulation

A switch is limited in the peak current \hat{I} and the input voltage U_{in} characterized in the datasheet (I_{Ref} and U_{Ref}). \hat{I} is calculated with the input power of the electric motor, the motor voltage U_{Motor} and the power factor $\cos\varphi$ of the inverter. If a design parameter exceeds a limit the modules of the inverter are further connected in series and/or parallel according to equation (26), where the parameter k_r represents an additional redundancy factor (brackets represent a round up to the next integer):

$$n_{parallel} = \left\lceil \frac{\hat{I}}{I_{Ref}} \right\rceil \cdot k_r; n_{Series} = \left\lceil \frac{\hat{U}}{U_{Ref}} \right\rceil \quad (26)$$

With $\hat{I} = \frac{P_{Design}}{\eta_{Motor} \cdot U_{Motor} \cdot \sqrt{3} \cdot \cos\varphi} \cdot \sqrt{2}$

Basically four losses occur in an inverter. In the transistor as well as in the diode conducting and switching losses occur. The conducting losses of the IGBT can be calculated with equation (27) taken from [24]:

$$P_{cond,IGBT} = \left(\frac{1}{2\pi} + \frac{\theta \cdot \cos(\varphi)}{8} \right) \cdot \frac{\hat{I}}{n_{parallel}} \cdot U_{CE0} + \left(\frac{1}{8} + \frac{\theta \cdot \cos(\varphi)}{3\pi} \right) \cdot \left(\frac{\hat{I}}{n_{parallel}} \right)^2 \cdot R_{CE} \quad (27)$$

$$\text{With } \theta = 2 \cdot \frac{\sqrt{3}}{3} \cdot \frac{U_{Motor}}{U_{In}}$$

$P_{cond,IGBT}$ is determined from the threshold voltage U_{CE0} and the forward slope resistance R_{CE} based on [24] as well as the peak output current through the collector \hat{I} . The parameter θ represents the modulation index taken from [27]. The switching losses $P_{sw,IGBT}$ of the IGBT can be calculated with equation (28) taken from [24]:

$$P_{sw,IGBT} = E_{Tr} \cdot \frac{\hat{I}}{I_{Ref}} \cdot \left(\frac{U_{In}}{U_{CE,Ref}} \right)^{1.4} \cdot f_{sw} \quad (28)$$

The switching energy E_{Tr} and switching times are not only dependent on the semiconductor itself, but also on the surroundings. Stray inductance, driver output or motor cable and

filter capacities affect the switching behavior as well. The data sheet values are therefore to be regarded as typical values only. The first term scales the sum of the switching energy (on and off) and multiplies it by the number of switches per second f_{sw} . Required f_{sw} is determined according to equation (29):

$$f_{sw} = n_{Motor} \cdot p \cdot k_p \quad (29)$$

n_{Motor} represents the maximum operating rotational speed of the electric motor, p the number of pole pairs and the factor k_p represents number of pulses generated by the controller per period. Because the switching loss estimation is only valid for $f_{sw} \gg n_{Motor}$ the parameter k_p was chosen to be 100 for all inverter designs. The conduction loss of the diode is similar to the IGBT and can be estimated with equation (30) taken from [28]:

$$P_{cond,Diode} = \left(\frac{1}{2\pi} - \frac{\theta \cdot \cos(\varphi)}{8} \right) \cdot \frac{\hat{I}}{n_{parallel}} \cdot U_{F0} + \left(\frac{1}{8} - \frac{\theta \cdot \cos(\varphi)}{3\pi} \right) \cdot \left(\frac{\hat{I}}{n_{parallel}} \right)^2 \cdot R_F \quad (30)$$

The switching losses of the diode are also similar to the IGBT and can be calculated with equation (31) from [24]:

$$P_{sw,Diode} = \frac{E_D}{\pi} \cdot \left(\frac{\hat{I}}{I_{F,Ref}} \right)^{0.6} \cdot \left(\frac{U_{In}}{U_{F,Ref}} \right) \cdot f_{sw} \quad (31)$$

The total inverter efficiency $\eta_{Inverter}$ can then be estimated with equation (32) by summing up all single losses and multiply the loss of one switch with the total number of switches installed.

$$\eta_{Inverter} = \frac{P_{Out}}{P_{In}} = \frac{P_{Out}}{P_{Out} + \sum_n P_n \cdot n_{series} \cdot n_{parallel}} \quad (32)$$

3.3.2 Mass Modeling

The mass is calculated by the number of power switches times the mass of one power switch. The number of power switches is calculated by the number of switches in parallel and switches in series times 6 (for each phase two modules). For additional equipment like housing, temperature conducting materials and mountings this mass is multiplied with $k_{Services}$

2.5 calibrated according to [29] as shown with equation (33):

$$m_{Switches} = (6 \cdot n_{parallel} \cdot n_{series} \cdot m_{Switch}) \cdot k_{Services} \quad (33)$$

The final controller mass is calculated with equation (34) considering also a cable mass factor k_{Cables} of 1.2 of the total switch mass calibrated according to [29]:

$$m_{Inverter} = m_{Switches} \cdot k_{Cables} \quad (34)$$

The reference parameters of the used power switch are summarized in Table 8 taken from [25].

Table 8: Reference values for inverter modelling adapted from [25]

Inverter Power Factor* $\cos(\varphi)$	1.0		
Min. Input Voltage* U_{In}	1.33 U_{Motor}^*		
Mass per switch m_{Switch}	330 g		
Transistor (IGBT)		Diode	
Switching Energy E_{Tr}	195 mJ	Switching Energy E_D	53 mJ
Threshold voltage**	0.8 V	Forward Voltage	2.64 V
U_{CE0}		$U_{F,Ref}$	
Continuous current* I_{Ref}	900 A	Threshold voltage	1.1 V
		U_{F0}	
Resistance* R_{CE}	1.8 m Ω	Forward current $I_{F,Ref}$	900 A
Max. Collector-Emitter Voltage $U_{CE,Ref}$	1200 V	Slope resistance R_F	1.71 m Ω
* parameters based on SemiSel online-tool Semikron [26] ** based on collector-emitter			

4 Results

The following section shows the validation of the derived models. Moreover, the component mass and efficiency figures obtained for the propulsion system of a universally electric medium-capacity, short-haul passenger aircraft are presented and discussed.

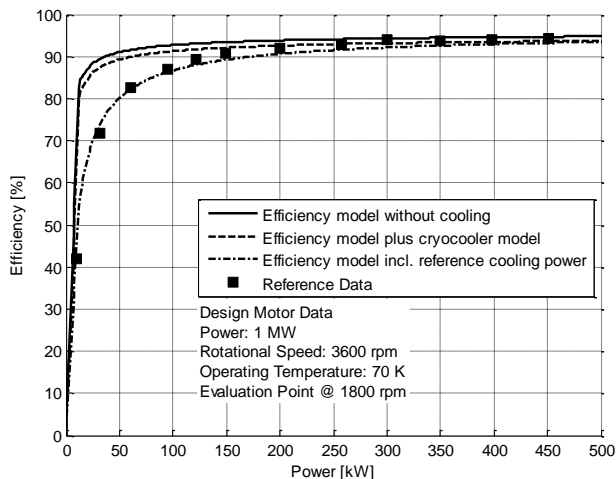
4.1 Validation of Electric Components

Table 9 shows the geometry and mass comparison of a conventional PMS motor at a design rotational speed of 5832 rpm and a design power of 40 kW taken from [16].

Table 9: Mass comparison of a conventional 40 kW PMS motor with 4 poles

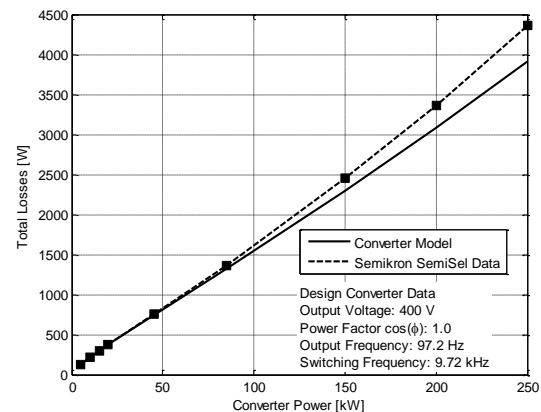
	Motor IPM-B' [16]	Model	Delta
Rotor Diameter [m]	0.18	0.18	0.0%
Rotor Length [m]	0.04	0.041	2.5%
Design Speed [rpm]	5832	5832	0.0%
Armature [kg]	5.0	4.9	-2.6%
Magnets [kg]	0.7	0.74	5.7%
Stator [kg]	9.0	9.2	2.4%
Rotor [kg]	4.2	5.0	19.0%
Total [kg]	18.9	22.4	18.5%

The error of the rotor active length is less than 2.5%. The error of the derived total mass is about 18.5%. This error is mainly the result of the rotor cross section calculation. Because the reference machine is a 4 pole machine the geometric impact on the rotor cross section is currently not represented by the model (full shaft). This is also the reason why the rotor mass is 19% higher compared to the reference. Furthermore, for this comparison the magnet angle of the baseline motor parameters was adapted to 27 deg and the stator yoke ratio to 0.48 to meet the outer motor diameter, which is valid in this case because the number of pole pairs are different.

**Fig. 4: Comparison of efficiency model of a HTS motor (only rotor) with reference data from [19]**

The efficiency in the motor design point is calculated with 91%. According to Carraro et.al. [16] the efficiency of the investigated machine is higher than 95%. The efficiency model

appears to over predict losses for conventional machines. Nevertheless, for HTS and full HTS motors the approach delivers the desirable accuracy due to the lapse of certain loss types as shown in Fig. 4. It shows the efficiency model (without cooling, with the reference cooling power of 7500 W and the cooling power calculated with methods described in Section 3.2) compared to the reference motor data for a certain off-design characteristic at 1800 rpm. The cryocooler model seems to under predict the cooling demand for low power demands. During higher power demands the estimated cooling power of the cryocooler is near the published cooling demand. Therefore, a constant cooling power is used (considering also heat conduction and radiation losses) where the error lies in a range between $\pm 2\%$. Fig. 5 shows the comparison of the developed converter efficiency model with the manufacturer's calculated data [26].

**Fig. 5: Comparison of converter model with manufacturer data [26]**

The maximum error of the losses is -10% at high power or electric current demands, which is mainly caused by the switching loss estimation. On total converter level the error is less than 0.5%.

4.2 Application Study

As reference system the Silent Advanced Fan utilizing Electrical Energy (SAFE) concept of the Ce-Liner serves as datum, which has a top-of climb thrust requirement of 33 kN and a take-off thrust requirement of 149 kN [4]. Accordingly, during OEI conditions the fan

requires a power of 22.2 MW at a rotational speed of 2000 rpm, which serves as sizing point of the electric propulsion system. Furthermore, a two stage planetary gearbox system is assumed between the fan and the electric motor. The efficiency was assumed to be 99.5% per stage and the mass is calculated according to methods published by Steiner et.al. [5]. For this configuration the optimal rotational speed was calculated to be 11000 rpm at a motor power during OEI of 22.4 MW. For this motor power and rotational speed the controller was designed with a redundancy factor of 2. The controller is supplied by a 3000 VDC system according to the published data [4]. The results of this approach are listed in Table 10 and compared to the original published data calculated with simplified methods.

Table 10: Mass and performance of the electric propulsion system of a shaft power demand of 22.2 MW of a ducted fan

	Datum [4]	Case Study	Delta [%]
Electric Motor Mass [kg]	1110	1423	28.2
Controller Mass [kg]	1240	1060	-14.5
Cryocooler Mass [kg]	149	100	-32.8
Gear Box System [kg]	345	379	9.9
Total Mass [kg]	2803	2872	2.5
Take-Off Performance (OEI)			
Electric Motor Efficiency* [%]	99.7	99.2	-0.5
Converter Efficiency [%]	99.5	99.9	0.4
Total Efficiency [%]	99.2	99.1	-0.1
Power losses and cooling demand during OEI			
Armature Losses [kW]	n/a	0.0	n/a
Stator Core Losses [kW]		25.7	
Stray Load Losses [kW]		46.8	
Friction Losses [kW]		45.1	
Miscellaneous [kW]		19.9	
Total Losses [kW]		137.5	
Cooling Power [kW]		34.3	
* incl. cooling			

It can be seen that with the refined and improved approach of this paper, the HTS motor mass is higher than the original published data with a specific power of 15.8 kW/kg. This value is also lower compared to data published by Brown [11] for full HTS motors. The higher

mass impact is also a result of the reduced operating speed of the electric motor from 35000rpm [4] to 11000 rpm. Also the calculated controller mass with a specific power of 21.3 kW/kg lies in good agreement with previous published data. Concerning the efficiency calculation the full HTS motor was estimated to be 99.2% including the cooling system, which is slightly lower than data published by Brown [11].

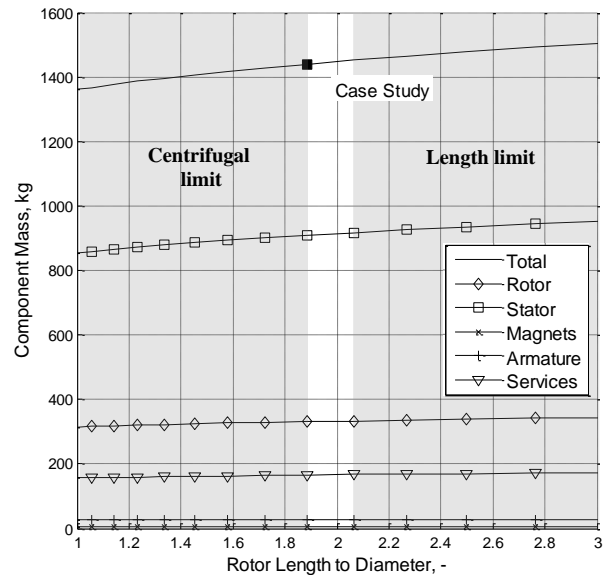


Fig. 6: Trade study of different rotor length to diameter variation at 22 MW and 11000 rpm

Fig. 6 shows a variation of the length to diameter ratio of the optimized motor design. It can be seen that at this high rotational speeds the motor has a small feasible bandwidth limited by centrifugal forces for ratios lower than 1.8 and for ratios higher than 2.05 limited by the rotor length. Furthermore, the design point shown in the diagram indicates that the design rotational speed is equal to the maximum rotational speed of the motor. Region II of the electric motor characteristic (cf. Figure 1) is typically not be reached during normal operation as torque increases monotonically with increasing power for propulsors with fixed blade pitch. Another interesting point is that the stator mass dominates the mass breakdown compared to the other components. This is the impact of the stator yoke ratio assumption, which was set constant to 0.6 (rotor radius to stator yoke height). Because the ratio depends

also on the pole pairs and the magnetic flux density a refinement of this assumption has to be conducted for further investigations. Furthermore, the rotor mass could also be reduced by refine the rotor geometry calculation for different pole pairs as mentioned before.

5 Conclusion and Outlook

In this paper a sizing approach for an electric motor, inverter and cryocooler system was presented. The developed method was applied on an electric ducted fan with a shaft power demand of 22.2MW at 2000 rpm. For these requirements an optimal motor design was identified at a motor speed of 11000 rpm with a specific power of 15.8 kW/kg and 99.2% efficiency and a controller design with 23 kW/kg and over 99.5% efficiency. For future work a wider design space with regard to thrust and rotational speed ranges is required to identify the optimum motor configuration for different aircraft classes. For this purpose the geometric relations have to be further refined especially regarding stator and rotor geometry also considering different pole pairs. Beside the stator yoke and rotor cross section the pole pairs have also an impact on the magnet angles. Furthermore, also the influence of different voltage levels and limitations of the electric motor has to be considered in future work.

Acknowledgments

The authors would like to thank U. Kling and Dr. A.T. Isikveren for valuable advice and fruitful discussions.

References

- [1] Bradley M, Droney C, Paisley D, Roth B, Gowda S, Kirby M. *NASA N+3 Subsonic Ultra Green Aircraft Research SUGAR Final Review*, Boeing Research and Technology, 2010.
- [2] Advisory Council for Aviation Research and Innovation in Europe. *Strategic Research & Innovation Agenda - Volume 1*, 2012.
- [3] Pernet C, Gologan C, Vratny PC, Seitz A, Schmitz O, Isikveren AT, Hornung M. *Methodology for Sizing and Performance Assessment of Hybrid Energy Aircraft*. Journal of Aircraft, pp 1–20, 2014.
- [4] Bauhaus Luftfahrt. *Initial Technical Assessment of an Electrically-powered, medium-capacity, Short-haul Transport Aircraft*. Bauhaus Luftfahrt, Technical Report, Munich, 2012.
- [5] Steiner H-J, Vratny PC, Gologan C, Wieczorek K, Isikveren AT, Hornung M. *Optimum number of engines for transport aircraft employing electrically powered distributed propulsion*. CEAS Aeronautical Journal, Vol. 5, pp 157-170, 2014.
- [6] Neudorfer H. *Weiterentwicklung von elektrischen Antriebssystemen für Elektro- und Hybridstraßenfahrzeuge*. 1st edition, Österreichischer Verband für Elektrotechnik, 2008.
- [7] Patel HK, Nagarsheth R, Parmerkar S. *Performance Comparison of Permanent Magnet Synchronous Motor and Induction Motor for Cooling Tower Application*. International Journal of Emerging Technology and Advanced Engineering, Vol. 2, pp 167–171, 2012.
- [8] Barnes P, Sumption M, Rhoads G. *Review of high power density superconducting generators: Present state and prospects for incorporating YBCO windings*. Cryogenics, Vol. 45, pp 670–686 2005.
- [9] Sivasubramaniam K, Zhang T, Lokhandwalla M, Laskaris ET, Bray JW, Gerstler B, Shah MR, Alexander JP. *Development of a High Speed HTS Generator for Airborne Applications*. IEEE Transactions on Applied Superconductivity, Vol. 19, pp 1656–1661, 2009.
- [10] Luongo CA, Masson PJ, Nam T, Mavris D, Kim HD, Brown GV, Waters M, Hall D. *Next Generation More-Electric Aircraft: A Potential Application for HTS Superconductors*. IEEE Transactions on Applied Superconductivity, Vol. 19, pp 1055–1068, 2009.
- [11] Brown G V. *Weights and Efficiencies of Electric Components of a Turboelectric Aircraft Propulsion System*. 49th AIAA Aerospace Sciences Meeting including the New Horizons Forum and Aerospace Exposition. Orlando, AIAA 2011-225, 2011.
- [12] Winternheimer S. *Skript zur Vorlesung Leistungselektronik I*. Lectural Note, 2007.
- [13] Pyrhönen J, Jokinen T, Hrabovocá V. *Design of Rotating Electrical Machines*. 2nd edition, John Wiley & Sons, Ltd., 2008.
- [14] Rucker JE. *Design and Analysis of a Permanent Magnet Generator for Naval Applications*. Master Thesis, Massachusetts Institute of Technology, 2005.
- [15] Bogomolov MD. *Concept study of 20 MW high-speed permanent magnet synchronous motor for marine propulsion*. Report 2013009, Eindverslag Stan Ackermans Intituuat ICT, 2013.
- [16] Carraro E, Degano M, Morandin M, Bianchi N. *Formula SAE Electric Competition : Electrical Motor Design*. Electric Machines & Drives Conference, Chicago, pp 1142–1148, 2013.
- [17] Lokhandwalla M, Haran KS, Alexander JP. *Scaling studies of high speed high temperature superconducting generator*. 2012 XXth International Conference of Electrical Machines, Marseille, pp 751–756, 2012.

- [18] Kalsi SS. *Applications of High Temperature Superconductors to Electric Power Equipment*. John Wiley & Sons, Inc., 2011.
- [19] Baik SK, Kwon YK, Kim HM, Kim SH, Lee JD, Kim YC, Park HJ, Kwon WS, Park GS. *Electrical parameter evaluation of a 1MW HTS motor via analysis and experiments*. Cryogenics, Vol. 49, pp 271–276, 2009.
- [20] Nick W, Grundmann J, Frauenhofer J. *Test Results from Siemens Low-Speed , High-Torque HTS Machine and Description of further Steps towards Commercialization of HTS Machines*. IEEE/CSC ESAS European Superconductivity News Forum, No. 19, pp 1-10, 2012.
- [21] Grune R. *Verlustoptimaler Betrieb einer elektrisch erregten Synchronmaschine für den Einsatz in Elektrofahrzeugen*. PhD Thesis, School IV-Electrical Engineering and Computer Science, 2012.
- [22] Binder A. *High speed PM machines*. Darmstadt, Lectural Note.
- [23] Seitz A, Isikveren AT, Hornung M. *Pre-Concept Performance Investigation of Electrically Powered Aero-Propulsion Systems*. Joint Propulsion Conference and Exhibit, San Jose, 2013.
- [24] Wintrich A, Nicolai U, Tursky W, Reimann T. *Application Manual Power Semiconductors*. ISLE Verlag, 2011.
- [25] SEMIKRON. *Datasheet SKM900GA12E4*. Datasheet, 2013.
- [26] SEMIKRON. *SEMIKRON / SemiSel 4.1*, Simulation Tool, URL:<http://semisel.semikron.com/circuit.asp>.
- [27] Sargos F. *IGBT Power Electronics Teaching System Principle for sizing power converters*. Application Note AN8005, 2008.
- [28] Mohr M, Fuchs FW. *Comparison of Three Phase Current Source Inverters and Voltage Source Inverters Linked with DC to DC Boost Converters for Fuel Cell Generation Systems*. European Conference on Power Electronics and Applications, pp 1-10, 2005.
- [29] Dvorský G. *HBC - SERIES V7 300400-3, 400400-3*. Manual, Zlin.

distribution of this paper as part of the ICAS 2014 proceedings or as individual off-prints from the proceedings.

Contact Author Email Address

patrick.vratny@bauhaus-luftfahrt.net

Copyright Statement

The authors confirm that they, and/or their company or organization, hold copyright on all of the original material included in this paper. The authors also confirm that they have obtained permission, from the copyright holder of any third party material included in this paper, to publish it as part of their paper. The authors confirm that they give permission, or have obtained permission from the copyright holder of this paper, for the publication and